

# Resonator-Aided Single-Atom Detection on a Microfabricated Chip

Igor Teper, Yu-Ju Lin, and Vladan Vuletić  
*MIT-Harvard Center for Ultracold Atoms, MIT, Cambridge, MA 02139.*  
(Dated: July 15, 2018)

We use an optical cavity to detect single atoms magnetically trapped on an atom chip. We implement the detection using both fluorescence into the cavity and reduction in cavity transmission due to the presence of atoms. In fluorescence, we register 2.0(2) photon counts per atom, which allows us to detect single atoms with 75% efficiency in 250  $\mu$ s. In absorption, we measure transmission attenuation of 3.3(3)% per atom, which allows us to count small numbers of atoms with a resolution of about 1 atom.

In the past several years, there have been many promising developments in the field of microfabricated magnetic traps (microtraps) for ultracold atoms, including experimental realizations of microtrap-based atom interferometers [1, 2], atomic clocks [3], and Bragg reflectors [4]. Compared to optical traps, where significant progress in interferometry [5], Josephson junctions [6] and one-dimensional physics [7, 8, 9] has been made, microchips offer smaller length scales and tighter confinement for single traps, which, however, may require working with small atom numbers. Furthermore, there are many proposed atom chip experiments, such as the implementation of a Tonks-Girardeau gas [10, 11] or an atomic Fabry-Perot interferometer [12] in a magnetic trap, that may greatly benefit from measuring atom statistics and correlations at the single-atom level, as has recently been demonstrated in a free-space experiment [13]. In addition, the preparation and detection of single atoms in microtraps constitute an important step toward quantum information processing with neutral atoms, which could take advantage of the tight, complex, precisely controlled, and scalable magnetic traps available on microchips [14]. In this context, the problem arises of how to detect small atom numbers in magnetic microtraps close to a substrate surface with a good signal-to-noise ratio [15, 16].

While cavity QED experiments [17, 18] can detect and count single atoms in the strong coupling regime, integrating very-high-finesse Fabry-Perot cavities with atom chips may prove difficult [16]. Observing small atom numbers through fluorescence in a magneto-optical trap (MOT) [19] or in MOT-loaded dipole traps [20, 21] requires long measurement times, and is also not easily compatible with chip traps. While experimental progress has recently been made in incorporating fiber resonators [22] and microcavities [23] into atom chips, the capabilities of such detection methods remain to be established. Recently, a low-finesse concentric cavity was used for sensitive detection of atoms in a macroscopic magnetic waveguide in a free-space geometry [24].

Atom detection can be implemented via fluorescence [19, 20, 21] or absorption methods [13, 17, 18]. To compare the two methods, consider a sample of  $a$  atoms, where each atom on average scatters  $m$  photons, and the imaging system detects a fraction  $\alpha$  of the photons. If background counts can be neglected, the atom number uncertainty  $\Delta a$  in fluorescence detection is given by

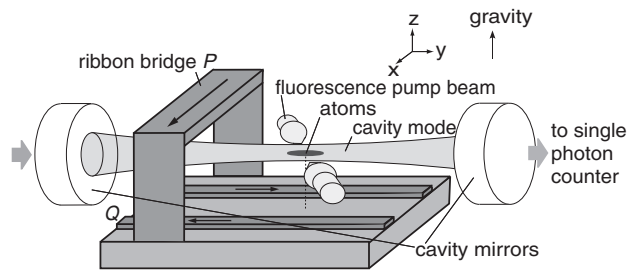


FIG. 1: Cavity and microfabricated chip (not to scale). The chip wires ( $Q$ ) generate a 2D quadrupole field in the  $xz$  plane. The ribbon ( $P$ ) in combination with an external field gradient creates the confinement along  $y$ . The atoms are probed either with a pump beam from the side to induce fluorescence into the cavity or through the absorption of a beam coupled through the cavity.

the ratio between the photon shot noise,  $\sqrt{a\alpha m}$ , and the signal per atom,  $\alpha m$ , and equal to  $\Delta a = \sqrt{a/\alpha m}$ . Consequently, in fluorescence measurements, the resolution decreases as the square root of the atom number.

For the equivalent absorption measurement, we assume the same number  $m$  of scattered photons per atom, an absorption beam matched to the collection optics, and low total absorption. Then, the number of incoming photons is  $m/\alpha$  with a shot noise  $\sqrt{m/\alpha}$ . This results in an atom number uncertainty of  $\Delta a = \sqrt{1/\alpha m}$ , independent of atom number and equal to the fluorescence resolution for  $a = 1$ . Thus, while fluorescence detection may provide a superior single-atom detector if background counts are negligible, absorption detection should perform better as a single-shot atom counter. Cavity-aided detection is attractive for both fluorescence and absorption methods, since the emission of light into the cavity is enhanced by the Purcell factor  $F/\pi$ , where  $F$  is the cavity finesse [25].

In this paper, we investigate the detection and counting of small numbers of atoms in a magnetic microtrap using a macroscopic, medium-finesse Fabry-Perot cavity employing both fluorescence and absorption detection techniques. Using shot-noise-limited atom preparation down to 1 atom, we achieve single-atom sensitivity in the fluorescence scheme, and a resolution of about 1 atom in absorption.

Our experimental setup (Fig. 1) is similar to that described in Ref. [26].  $^{87}\text{Rb}$  atoms are trapped and cooled in a free-space magneto-optical trap, transferred to a magnetic trap, which is then moved close to the chip and adiabatically transformed into a Ioffe-Pritchard microtrap. The radial ( $xz$ ) confinement of the chip trap is provided by two 2- $\mu\text{m}$ -high, 500- $\mu\text{m}$ -wide gold wires  $Q$ , whose centers are separated by 1 mm, carrying antiparallel currents along the  $y$  direction, in superposition with a bias field along  $z$ . The axial ( $y$ ) confinement is created by a current through a gold ribbon bridge  $P$  along  $x$ , 500  $\mu\text{m}$  away from the chip's surface, in combination with an external field gradient along  $y$ . We have mounted high-reflectivity, low-loss mirrors on opposite sides of the chip to form a 2.66 cm long near-confocal cavity with  $\text{TEM}_{00}$  mode waist  $w$  of 56  $\mu\text{m}$ , finesse  $F = 8600$ , linewidth  $\kappa/2\pi = 650$  kHz, free spectral range of 5630 MHz, and transverse mode spacing of 230 MHz, aligned along the axis of our magnetic trap and located 200  $\mu\text{m}$  away from the chip surface, so that the cavity mode passes between the bridge bond and the chip. The mode waist is displaced longitudinally by 5.6 mm relative to the microtrap. For the fluorescence measurement, a retroreflected pump beam with a waist of 250  $\mu\text{m}$  at the position of the atoms is coupled from the side of the cavity at an angle of 70° to the cavity axis.

We prepare our atoms by initially loading them into a Ioffe-Pritchard microtrap located 200  $\mu\text{m}$  away from the surface and displaced to the side of the cavity axis in order to prevent them from being heated by the cavity length stabilization light. We then use a fast radiofrequency (RF) evaporation to remove the vast majority of the atoms, leaving us with a small number of cold atoms at a typical temperature of 15  $\mu\text{K}$ . Once we have the sample ready, we ramp the magnetic field to move the trap into the cavity mode, turn off the locking light, and perform the fluorescence or absorption measurement. When located in the cavity, the magnetic trap has a radial gradient of 200 G/cm, which corresponds to transverse vibration frequencies around 300 Hz for typical offset fields, and an axial vibration frequency of 50 Hz.

Using optics outside the vacuum chamber, we couple up to 95% of the light entering the cavity into the  $\text{TEM}_{00}$  mode. The light exiting the cavity is mode-matched to a single-mode fiber, which allows for excellent spatial filtering of background light, and delivered to a single-photon-counting module (SPCM). We stabilize our cavity to an off-resonant laser of a linewidth slightly broader than that of the cavity using a Pound-Drever-Hall scheme. The stability of our cavity lock is  $140$  kHz/ $\sqrt{10\text{kHz}}$  for a locked cavity, and  $400$  kHz/ $\sqrt{10\text{kHz}}$  in the several ms after the locking light is extinguished, which is when we perform our measurements.

Both absorption and fluorescence signals in cavity-aided detection depend on the atoms' scattering rate of photons into the cavity. For an atom on the cavity axis, the ratio  $\eta$  of its scattering rate into each of the two directions of the cavity,  $\Gamma_c$ , to its scattering rate into

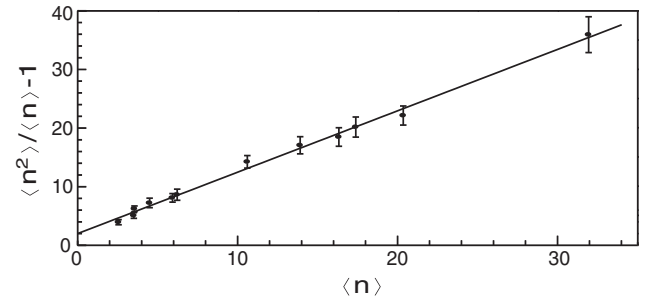


FIG. 2: Characterization of the atom number preparation noise and detected photon number per atom for fluorescence detection.  $n$  denotes the number of signal photons detected. The atom-atom correlation function,  $g_{aa}$ , is given by the slope, and the average number of photon counts per atom,  $\langle p \rangle$ , is given by the y-axis intercept.

free space,  $\Gamma_s$ , is given by the single-atom cooperativity,  $\eta = 6F/(\pi(wk)^2)$ , where  $w$  is the cavity mode waist size and  $k = 2\pi/\lambda$  with  $\lambda$  as the optical wavelength resonant with the cavity mode; for our cavity,  $\eta = 0.07$ . To confirm our atom-cavity coupling experimentally, we measure the tuning of the transmission resonance by samples large enough that the atom number can be determined by standard absorption techniques. The tuning of the cavity resonance by an atom well-localized at the cavity waist is given by  $\delta\nu = (\kappa/2)(\Gamma/\Delta)N\eta$ , where  $\Gamma$  is the linewidth of the atomic transition,  $\Delta \gg \Gamma$  is the detuning between the laser and the atomic transition, and  $N$  is the atom number. The measurement of  $\delta\nu$  yields a value of  $\eta$  between 0.015 and 0.025, in good agreement with the value we would expect given our independent measurement of the cloud size, which reduces  $\eta$  compared to the on-axis case.

To characterize both the atom number preparation and the number of photon counts per atom in fluorescence detection, we illuminate the atoms with a near-resonant pump beam just above saturation and count the photons emerging from the cavity within 750  $\mu\text{s}$ . We compile histograms of counts for different RF final settings, i.e., different average numbers of prepared atoms. Given Poisson statistics for the detected photons, the following relation can be derived:  $\langle n^2 \rangle / \langle n \rangle - 1 = g_{aa} \langle n \rangle + \langle p \rangle$ , where  $\langle a \rangle$  is the mean atom number,  $\langle p \rangle$  is the mean number of photon counts per atom,  $n = ap$  is the number of signal photon counts, and  $g_{aa}$  is the atom-atom correlation function, which should be equal to 1 if the atoms strictly obey Poisson statistics and equal to  $(1 + f^2)$  in the presence of (technical) fractional atom number noise of magnitude  $f$ . The values of  $\langle n^2 \rangle / \langle n \rangle - 1$  can be computed from each histogram independently without any knowledge about  $\langle a \rangle$  or  $\langle p \rangle$ , given that we can measure the background count rate independently, and assuming that fluctuations in the background are uncorrelated with fluctuations in the signal. The results, along with a linear fit, are plotted in Fig. 2. The fit gives a slope of

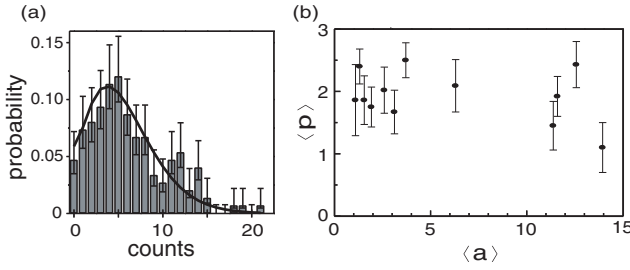


FIG. 3: (a) Typical normalized histogram of 150 fluorescence measurements, with Poisson fit to  $\langle a \rangle$ , the mean number of atoms, and  $\langle p \rangle$ , the mean number of photon counts per atom. In this case,  $\langle a \rangle = 3.1(4)$  and  $\langle p \rangle = 1.7(3)$ . Error bars are Poissonian uncertainties. (b) Results of Poisson fits to 12 different histograms, with error bars corresponding to 1 standard deviation in  $\langle p \rangle$ .

$g_{aa} = 1.05(2)$ , which implies that the fractional noise on our signal is  $0.25(10)$ , and therefore Poissonian fluctuations dominate for the atom numbers we measure, and an intercept of  $\langle p \rangle = 1.9(3)$ .

Having confirmed the Poisson statistics of our atom number preparation, we can fit the  $\langle a \rangle$  and  $\langle p \rangle$  for each histogram individually. A typical histogram with fit and a plot of the combined results of all histogram fits are shown in Fig. 3. To a good approximation, the average number of photon counts per atom is independent of atom number at  $\langle p \rangle = 2.0(2)$  counts/atom, with 0.3 background counts. An average of the signal time traces yields a  $1/e$  time of  $\tau = 150 \mu\text{s}$ .

Since our cavity resonance is much narrower than the atomic line, the cavity collects predominantly the coherently scattered photons and only a small fraction of the Mollow triplet [27]. The number of photon counts we would expect to detect per atom is thus given by  $\langle p \rangle = \Gamma_{coh}\tau\eta(\kappa/\gamma) \times CG \times g \times f \times q \times l$ , where  $\Gamma_{coh} = \Gamma/8 = 2\pi \times 760 \text{ kHz}$  is the maximum coherent scattering rate for the transition,  $\eta = 0.07$ ,  $\gamma = 2\pi \times 1 \text{ MHz}$  is the linewidth of the cavity transmission, which is a convolution of the cavity and laser linewidths,  $CG = 0.3$  is the averaged Clebsch-Gordan coefficient for  $\sigma^+$  intracavity light coming from the scattering process (the other polarizations are not resonant with the cavity),  $g = 0.6$  accounts for the finite size of the atomic cloud,  $f = 0.7$  is the coupling efficiency into the single-mode fiber,  $q = 0.58$  is the quantum efficiency of the SPCM, and  $l = 0.7$  is the signal reduction due to measured mechanical cavity vibrations. The combination of the above factors predicts  $\langle p \rangle = 1.7$ , close to our measured value.

In order to quantify the performance of our fluorescence measurement as a single-atom detector, we reduced the measurement window to  $250 \mu\text{s}$ , and took a histogram with, on average, less than one atom prepared. The Poisson fit to the resulting histogram gives  $\langle a \rangle = 0.85(8)$  and  $\langle p \rangle = 1.4(1)$ . Combined with a measured background of 0.07 counts, this means that, if we set our detection threshold to  $\geq 1$  count, our single-atom detection is char-

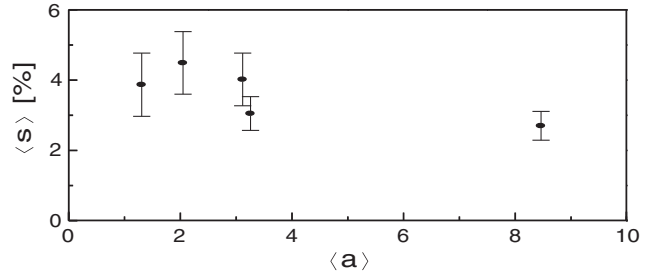


FIG. 4: Results of Poisson fits to  $\langle s \rangle$ , the mean single-atom absorption, and  $\langle a \rangle$ , the mean atom number, for 5 different histograms.

acterized by an atom quantum efficiency of 75% and a false detection rate of 7%, at a maximum single-atom count rate of 4 kHz.

While the fluorescence measurement makes a good single-atom detector, we expect an absorption measurement to provide better atom number resolution for  $a > 1$ . For absorption detection, we couple the probe laser beam into the cavity  $\text{TEM}_{00}$  mode and monitor the resonant transmission through the cavity in the presence of atoms. The laser linewidth is broadened by frequency modulation to 30 MHz, much wider than  $\kappa$ , so that the intensity noise on the cavity transmission due to cavity vibration is negligible compared to the photon shot noise. The laser is tuned to atomic resonance with an intracavity saturation parameter equal to 0.2. The expected transmission reduction due to one atom of a laser resonant with the atomic transition is  $2\eta$ . Similarly to fluorescence detection, we compile histograms for different sets of atom preparation parameters and fit them, assuming Poisson statistics for both the atoms and the photons, to determine the mean absorption per atom,  $\langle s \rangle$ , and the mean atom number,  $\langle a \rangle$ . (A correlation function fit similar to the one for fluorescence confirms that our atom preparation for absorption has Poisson statistics, with  $g_{aa} = 0.94(4)$ .) The fitting results for  $\langle s \rangle$  with varying atom number are shown in Fig. 4. From these measurements, we obtain  $\langle s \rangle = 3.3(3)\%$  for  $1 < \langle a \rangle < 10$ , in good agreement with the expected absorption per atom,  $\langle s \rangle = 3.2(7)\%$ , when geometric factors due to finite cloud size are taken into account.

Using the measured values of  $\langle p \rangle = 2.0(2)$  counts/atom for fluorescence detection and  $\langle s \rangle = 3.3(2)\%$  for absorption, we can evaluate how well these two methods can determine the atom number in a single measurement. The expected atom number uncertainty  $\delta a$  using fluorescence (absorption) detection due to both photon shot noise and the statistical uncertainty in the mean number of photons per atom,  $\langle p \rangle$  (uncertainty in the mean absorption per atom,  $\langle s \rangle$ ), as well as the background photon counts (for fluorescence only), is plotted as a function of atom number in Fig. 5; the figure also includes a computed normalized histogram that characterizes the single-atom detection capability of our fluorescence mea-

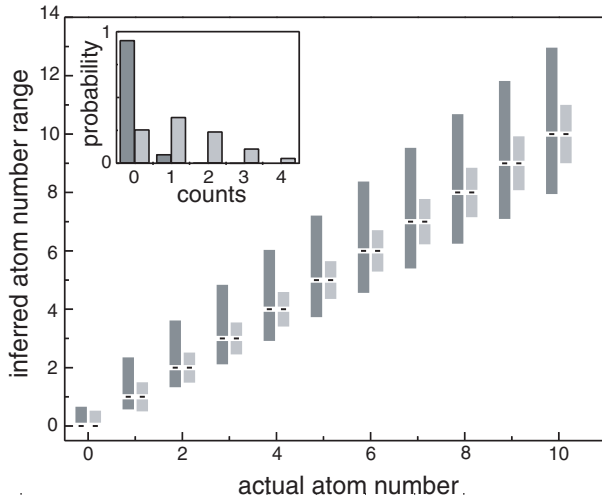


FIG. 5: Atom number measurement  $1-\sigma$  confidence intervals in a single shot for fluorescence ( $\tau = 750 \mu\text{s}$ , dark grey) and absorption ( $\tau = 1 \text{ ms}$ , light grey) measurements. The inset shows a computed normalized photon count distribution due to background counts (dark grey) and due to photons collected from one atom (light grey) for fluorescence single-atom detection ( $\tau = 750 \mu\text{s}$ ).

surement. For fluorescence, the atom number resolution is limited by the shot noise of the collected signal photons, which grows with atom number, while, for absorption, where the number of collected photons actually decreases with atom number, the resolution remains nearly

flat, at around 1 atom.

The demonstrated excellent atom number resolution could be useful in a variety of microchip experiments. For instance, a Tonks-Girardeau (TG) gas could be created close to the chip, where high radial vibration frequencies can be achieved. The sample could then be moved into the cavity to measure both the atom number and the density distribution of the gas. As an example, a quantum degenerate gas of 50  $^{87}\text{Rb}$  atoms confined in a magnetic trap with a radial trapping frequency of 20 kHz and an axial frequency of 0.5 Hz would be deep in the TG regime, with  $\gamma = 2/(n|a_{1D}|)$  of 10, where  $\gamma \gg 1$  means that the gas experiences strong fermionization, for a peak one-dimensional number density  $n$  and an effective one-dimensional scattering length  $a_{1D}$  [11]. Then the spatial ( $30 \mu\text{m}$ ) and atom number resolution of our detector would allow one to distinguish the length and density distribution of this TG gas ( $l = 300 \mu\text{m}$ ) from a corresponding non-fermionized Thomas-Fermi gas with the same atom number ( $l = 420 \mu\text{m}$ ).

In conclusion, we have demonstrated *in situ* detection of magnetically trapped atoms on a chip with the aid of a medium-finesse macroscopic cavity, and characterized the performance for single-atom detection and for atom number measurements using both fluorescence and absorption methods. We believe that, due to their combination of versatility, performance, and ease of use, such cavity-aided detection schemes can play an important role in a broad range of applications in integrated atom optics on chips.

This work was supported by the NSF and DARPA.

---

[1] Y.-J. Wang, D. Z. Anderson, V. M. Bright, E. A. Cornell, Q. Diot, T. Kishimoto, M. Prentiss, R. A. Saravanan, S. R. Segal, and S. Wu, Phys. Rev. Lett. **94**, 090405 (2005).  
[2] T. Schumm, S. Hofferberth, L. M. Andersson, S. Willemerth, S. Groth, I. Bar-Joseph, J. Schmiedmayer, and P. Krüger, Nature Physics **1**, 57 (2005).  
[3] P. Treutlein, P. Hommelhoff, T. Steinmetz, T. W. Hänsch, and J. Reichel, Phys. Rev. Lett. **92**, 203005 (2004).  
[4] A. Günther, S. Kraft, M. Kemmler, D. Koelle, R. Kleiner, C. Zimmermann, and J. Fortágh, Phys. Rev. Lett. **95**, 170405 (2005).  
[5] Y. Shin, M. Saba, T. A. Pasquini, W. Ketterle, D. E. Pritchard, and A. E. Leanhardt, Phys. Rev. Lett. **92**, 050405 (2004).  
[6] M. Albiez, R. Gati, J. Fölling, S. Hunsmann, M. Cristiani, and M. K. Oberthaler, Phys. Rev. Lett. **95**, 010402 (2005).  
[7] B. L. Tolra, K. M. O'Hara, J. H. Huckans, W. D. Phillips, S. L. Rolston, and J. V. Porto, Phys. Rev. Lett. **92**, 190401 (2004).  
[8] B. Paredes, A. Widera, V. Murg, O. Mandel, S. Fölling, I. Cirac, G. V. Shlyapnikov, T. W. Hänsch, and I. Bloch, Nature (London) **429**, 277 (2004).  
[9] T. Kinoshita, T. Wenger, and D. S. Weiss, Phys. Rev. Lett. **95**, 190406 (2005).  
[10] M. Olshanii, Phys. Rev. Lett. **81**, 938 (1998).  
[11] V. Dunjko, V. Lorent, and M. Olshanii, Phys. Rev. Lett. **86**, 5413 (2001).  
[12] I. Carusotto, Phys. Rev. A **63**, 023610 (2001).  
[13] A. Öttl, S. Ritter, M. Köhl, and T. Esslinger, Phys. Rev. Lett. **95**, 090404 (2005).  
[14] T. Calarco, E. A. Hinds, D. Jaksch, J. Schmiedmayer, J. I. Cirac, and P. Zoller, Phys. Rev. A **61**, 022304 (2000).  
[15] P. Horak, B. G. Klappauf, A. Haase, R. Folman, J. Schmiedmayer, P. Domokos, and E. A. Hinds, Phys. Rev. A **67**, 043806 (2003).  
[16] R. Long, T. Steinmetz, P. Hommelhoff, W. Hänsel, T. W. Hänsch, and J. Reichel, Phil. Trans. R. Soc. Lond. A **361**, 1375 (2003).  
[17] P. Münstermann, T. Fischer, P. W. H. Pinkse, and G. Rempe, Opt. Comm. **159**, 63 (1999).  
[18] J. McKeever, J. R. Buck, A. D. Boozer, and H. J. Kimble, Phys. Rev. Lett. **93**, 143601 (2004).  
[19] C.-S. Chuu, F. Schreck, T. P. Meyrath, J. L. Hanssen, G. N. Price, and M. G. Raizen, Phys. Rev. Lett. **95**, 260403 (2005).  
[20] N. Schlosser, G. Reymond, I. Protsenko, and P. Grangier, Nature (London) **411**, 1024 (2001).

- [21] S. Kuhr, W. Alt, D. Schrader, M. Müller, V. Gomer, and D. Meschede, *Science* **293**, 278 (2001).
- [22] P. A. Quinto-Su, M. Tscherneck, M. Holmes, and N. P. Bigelow, *Opt. Express* **12**, 5098 (2004).
- [23] M. Trupke, E. A. Hinds, S. Eriksson, E. A. Curtis, Z. Moktadir, E. Kukharenka, and M. Kraft, *Appl. Phys. Lett.* **87**, 211106 (2005).
- [24] A. Haase, B. Hessmo, and J. Schmiedmayer, *Opt. Lett.* **31**, 268 (2006).
- [25] E. M. Purcell, *Phys. Rev.* **69**, 681 (1946).
- [26] Y. Lin, I. Teper, C. Chin, and V. Vuletić, *Phys. Rev. Lett.* **92**, 050404 (2004).
- [27] B. R. Mollow, *Phys. Rev.* **188**, 1969 (1969).